Title

A hydrologic feature detection algorithm to quantify seasonal components of flow regimes

Authors

Patterson, NK
Lane, BA
Sandoval-Solis, S
et al.

Publication Date

2020-06-01

DOI

10.1016/j.jhydrol.2020.124787

Peer reviewed

A hydrologic feature detection algorithm to quantify seasonal components of flow regimes

Noelle K. Patterson[1]*, Belize A. Lane[2], Samuel Sandoval-Solis[1], Gregory B. Pasternack[1], Sarah M. Yarnell[3], Yexuan Qiu[1]

*Corresponding author

Email: nkpatterson@ucdavis.edu

1. Department of Land, Air and Water Resources, University of California, Davis
2. Department of Civil and Environmental Engineering, Utah State University
3. Center for Watershed Sciences, University of California, Davis

Cite as:

Patterson, N. K., Lane, B. A., Sandoval-solis, S., Pasternack, G. B., Yarnell, S. M., & Qiu, Y. (2020). A hydrologic feature detection algorithm to quantify seasonal components of flow regimes. *Journal of Hydrology*, *585*, 1–12. https://doi.org/10.1016/j.jhydrol.2020.124787

The final version of this manuscript is available at ResearchGate at:
https://doi.org/10.1016/j.jhydrol.2020.124787

Highlights

- A new signal processing algorithm identifies seasonal transitions from daily flow data.
- Application to 223 unimpaired gages in California highlights algorithm performance.
- Algorithm identifies statistically distinct seasonal timing across diverse flow regimes.

Abstract

Seasonal flow transitions between wet and dry conditions are a primary control on river conditions, including biogeochemical processes and aquatic life-history strategies. In regions like California with highly seasonal flow patterns and immense interannual variability, a rigorous approach is needed to accurately identify and quantify seasonal flow transitions from the annual flow regime. Drawing on signal processing theory, this study develops a transferable approach to detect the timing of seasonal flow transitions from daily streamflow time series using an iterative smoothing, feature detection, and windowing methodology. The approach is shown to accurately identify and characterize seasonal flows across highly variable natural flow regimes in California. A quantitative error assessment validated the accuracy of the approach, finding that inaccuracies in seasonal timing identification did not exceed 10%, with infrequent exceptions. Results for seasonal timing were also used to highlight the statistically distinct timing found across streams with varying climatic drivers in California. The proposed approach improves understanding of spatial and temporal trends in hydrologic processes and climate conditions across complex landscapes and informs environmental water management efforts by delineating timing of seasonal flows.

Keywords

Streamflow hydrology, environmental flows, time series analysis, California

1. Introduction

Streams and rivers in semi-arid/Mediterranean climates are physically, chemically, and biologically driven by predictable, seasonal periods of wet and dry conditions over an annual cycle (Gasith and Resh, 1999). Seasonal flow regimes support predictable river processes such as disturbance regimes (Rood et al., 2005), seasonal habitat provision (Aadland, 1993, Booker and Acreman, 2007, Jacobson, 2013), and native species life-history cues (Yarnell et al., 2010). While streamflow characteristics including magnitude, duration, frequency, and rate of change are useful for describing components of the flow regime (Poff et al., 1997), the timing of seasonal flow transitions within the annual flow regime is particularly important for understanding seasonally-adapted ecological processes such as migration, spawning, or vegetation recruitment (Cambray, 1991, Greet et al., 2011, Poff and Zimmerman, 2010). It is critical to identify these distinct wet and dry conditions and when they occur across different flow regimes to improve understanding of physical climate and watershed controls on these seasonal transitions and their sensitivity to change.

Numerical descriptors of the flow regime, known as flow metrics, are routinely quantified from daily streamflow time series to link streamflow patterns to river processes (Buttle, 2011, Poff and Ward, 1989) and biological response (Mazor et al., 2017, Olden and Poff, 2003). Existing flow metrics used to identify and quantify the timing of seasonal flow transitions are limited, especially across large regions and in hydrologically variable settings. These measurements of timing are often simplified by calculating flow metrics within predetermined timing windows instead of identifying the occurrence of seasonal transitions and key events based on annual flow patterns. The Hydroecological Integrity Assessment Process (Henriksen et al., 2006) and the Indicators of Hydrologic Alteration (Richter et al., 1996) incorporate timing through calculations such as monthly average flows or the date of annual minimum and maximum flow. However, in variable flow regimes such as flashy rain-sourced streams, the timing of seasonal flow transitions varies significantly between water years and hydroclimatic settings (Lane et al., 2018). This wide inter-annual variability suggests that metrics describing a particular aspect of seasonal flow, such as dry season flow magnitude, cannot be accurately quantified based on the same months in each water year. Calculation of the annual maximum or minimum

similarly may oversimplify understanding of seasonal flow components, because these calculations do not account for annual or seasonal patterns of flow or events other than the most extreme conditions (Déry et al., 2009).

To better quantify flow regimes based on variable seasonal patterns, signal processing techniques can be used to identify sub-annual hydrologic patterns from daily flow time series. Signal processing theory provides well-established techniques, such as data smoothing, peak detection, and time windowing, that have been applied in hydrology (Kusche et al., 2009, Mann, 2004) and can be used to detect features from a time series of daily streamflow data. Time series smoothing is used to enhance certain frequencies (i.e., the signal) while attenuating others (i.e., the noise), and many smoothing techniques are available such as moving average, exponential moving average, empirical mode decomposition, regression smoothing (e.g. LOESS, Cleaveland and Loader, 1996), wavelet, and splines (Janert, 2010). Smoothing functions generate fitted curves to time series data that emphasize different frequency signals depending on the function and level of smoothing (Pollock, 1999). Feature detection is used to extract peaks or valleys of interest from the smoothed data and can depend on attributes such as magnitude or slope (Schneider, 2011, Scholkmann et al., 2012). Dynamic windowing around a detected feature constrains further analysis to a particular period of interest and allows for increased resolution of subsequent analysis (Palshikar, 2009).

In previous work, signal processing techniques have been applied to hydrologic time series for applications such as detecting long-term trends (Letcher et al., 2001), modeling hydrologic processes (Zhang et al., 2016), and predicting future trends (Adamowski and Sun, 2010, Cannas et al., 2006). Common techniques such as harmonic analysis using Fourier or wavelet transform methods can be effective in analyzing hydrologic time series characteristics, such as periodicity, trends, coherence and cross-phase among deriving and response variables, or complexity determined by wavelet entropy (Pasternack and Hinnov, 2003, Sang, 2013). Additionally, many techniques have been developed to identify baseflow recession (Hall, 1968); recent attempts include identifying a consecutive number of days of negative slope in the hydrograph (Bart and Hope, 2014), combining requirements of negative slope with a percentile-based magnitude threshold (Sawaske and Freyberg, 2014), or automatic identification of recession curves based on parameters balancing accuracy and coverage (Smith and

Schwartz, 2017). While some methods share similarities with components of the proposed method, to the authors' knowledge there has not yet been a method developed to automatically isolate and quantify all major seasonal flow transitions from annual streamflow time series.

To identify ecologically significant flow transitions from the annual hydrograph, this study applied signal processing methods to identify functional flows found in the highly seasonal Mediterranean streams of California, USA. Functional flows refer to sub-annual aspects of the flow regime that support key ecological, geomorphic or biogeochemical processes in riverine systems (Escobar-Arias and Pasternack, 2010, Yarnell et al., 2015). Yarnell et al. (2015) aggregated flow ecology literature to identify four functional flow components relevant to Mediterranean streams with a distinct wet and dry season: wet-season initiation flows, peak magnitude flows, spring recession flows, and dry-season low flows. Building on those efforts and more recent work highlighting key functional flows specific to California (Yarnell et al., 2020), this study identifies the timing of four functional flow components applicable to California's natural streamflow regimes: fall pulse flow, wet season flow (encompassing both wet season baseflow and peak flow conditions), spring recession, and dry season baseflow (Fig. 1). Once the timings of functional flow transitions are identified from the annual hydrograph, each functional flow component can be further quantified using additional flow metrics such as magnitude, timing, frequency, duration, or rate of change, and can be used to design functional flow regimes in managed river systems (Yarnell et al., 2020).

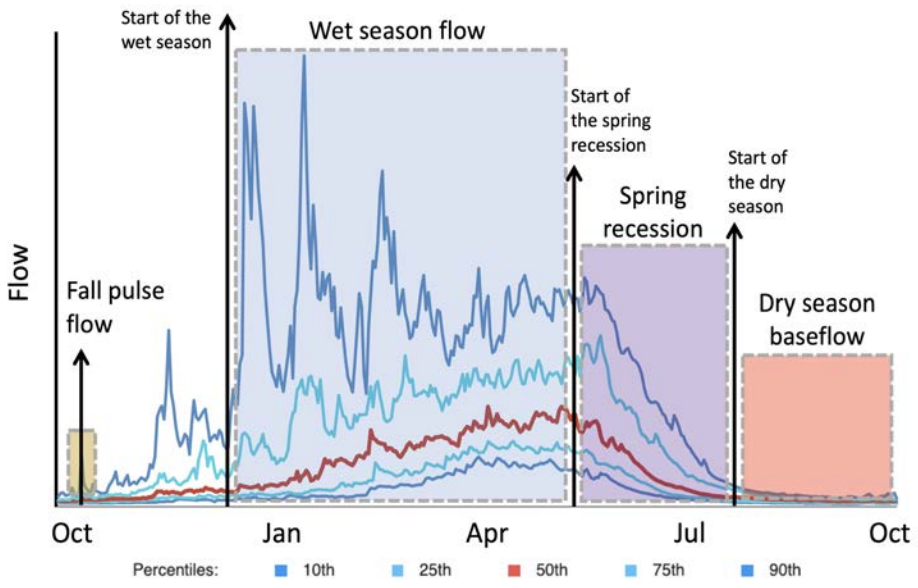

Fig. 1. Identification of the start timing of four functional flows identified for California (Yarnell et al., 2020) using the proposed signal processing algorithm. The timing of flow transitions identified by the algorithm are marked with arrows. Hydrographs indicate the 10th, 25th, 50th, 75th, and 90th percentiles of flow in a mixed rain-snow river system (modified from Yarnell et al., 2020). A water year in California is defined as October 1 to September 30.

Drawing on signal processing theory, this study develops an algorithm in the open-source Python programming language to calculate the timing of seasonal flow transitions from daily flow time series, allowing for improved characterization of seasonal flows. This research addresses the following questions: (1) is it possible to automatically identify timing of seasonal streamflow components from annual hydrographs, and if so what is the level of error?; and (2) does the timing of seasonal flow components calculated through this study reveal distinctions among streams with varying climatic drivers? Using data from the highly seasonal streams of California as a testbed, this study assesses the accuracy and limitations of the algorithm for quantifying functional flows across a wide range of natural flow regimes and climate conditions, including flow regimes exhibiting snowmelt, rain, or mixed rain and snowmelt signatures. To further achieve confidence in the results, algorithm outputs are analyzed in the context of California hydrology and tested for the extent that results align with expectations for regional hydrologic regimes.

2. Methods

The study design describes development, calibration, and performance assessment of the algorithm for detecting the timing of functional flow transitions from daily streamflow time series, with algorithm steps summarized in Fig. 4.

2.1. Study region

California has a Mediterranean climate with pronounced wet and dry seasons, as well as high interannual variability and spatial heterogeneity (Dettinger et al., 2011, Liu et al., 2018). Much of this variability stems from California's wide latitudinal extent (800 km) and physiographic diversity, with

multiple mountain ranges and valleys of different sizes, shapes, and relief (Abatzoglou et al., 2009, LaDochy et al., 2007). California rainfall is characterized by the capability of a limited number of high intensity storm events to contribute to the majority of annual precipitation; Dettinger et al. (2011) found that 20–50% of California's long-term rainfall average derives from these high precipitation storm events. California's rivers and streams reflect the state's climatic and physiographic diversity, ranging from small, intermittent streams in the southwest deserts to larger snowmelt-fed rivers draining the western slopes of the Sierra Nevada mountain range (Lane et al., 2018, Mount, 1995).

For this study, nine natural hydrologic classes previously identified for California by Lane et al. (2018) were aggregated into three dominant stream types recognized throughout the state (Mount, 1995): snowmelt-, rainfall-, and mixed snowmelt and rain-sourced streams (Fig. 2). Snowmelt-sourced flow regimes are largely controlled by the timing and rate of snowmelt, which are driven by seasonal patterns of precipitation and temperature. Rain-sourced flow regimes are controlled by the intensity of winter rainfall and characteristics of individual storm events. Mixed-source streams experience both rain-driven flows in the winter and a snowmelt pulse in the spring, or they occur in large drainages that receive both snowmelt and rainfall contributions from upstream.

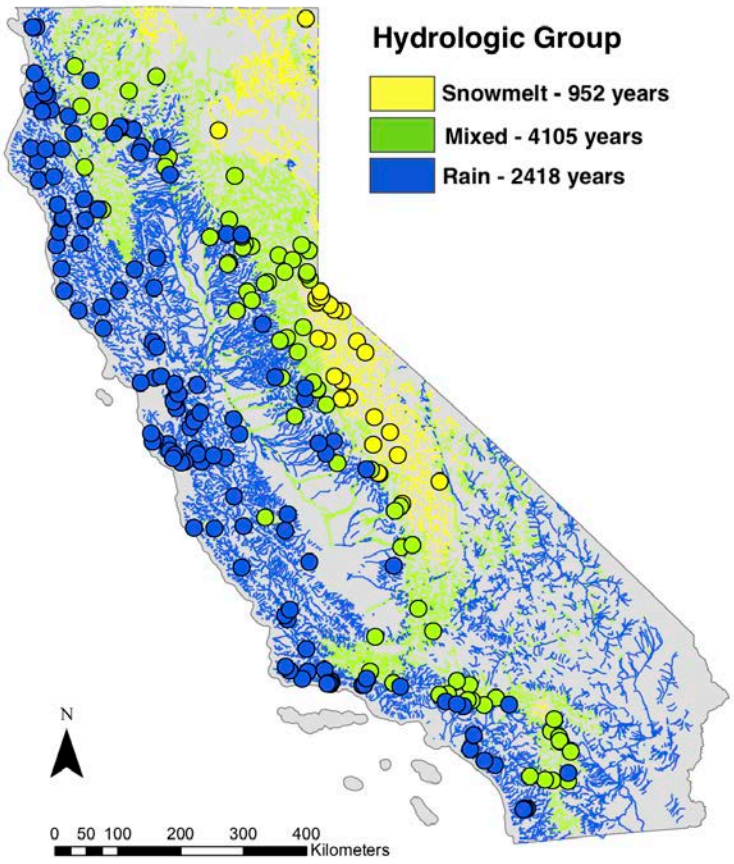

170

171 Fig. 2. The three dominant stream types in California based on aggregated natural hydrologic classes
172 developed by Lane et al. (2018): snowmelt (yellow), mixed snow and rain (green), and rain (blue).
173 Reference streamflow gages used in this study are shown as circles, and the number of total water
174 years of data in each stream type are shown. (For interpretation of the references to colour in this
175 figure legend, the reader is referred to the web version of this article.)

176

2.2. Data

Streamflow data used for this analysis come from 223 gage stations with unimpaired or naturalized daily streamflow records in California (refer to Kennard et al., 2010 for definitions of unimpaired and naturalized streamflow) (Fig. 2). Unimpaired gage data was sourced from the dataset compiled by Zimmerman et al. (2017), who followed a 3-step protocol to obtain unimpaired daily streamflow. Their process designated gage stations as unimpaired based on: (1) designation as a "least disturbed" site from a U.S. Geological Survey database of watershed attributes (Falcone et al., 2010), (2) status of unimpairment based on annual gage station reports and appearance of natural conditions from satellite imagery, and (3) historical flow records that pre-date anthropogenic disturbance such as dams and urbanization. Seven gages with simulated unimpaired (i.e., naturalized) daily streamflow data were also added to the dataset to cover the Central Valley region of California (CDWR, 2007), which was otherwise poorly represented by unimpaired gage stations. A final screening of the annual hydrographs of the resulting dataset was performed, and several gages were removed from the analysis that had flow patterns appearing irregular, impaired, or too low to exhibit seasonal patterns. The resulting dataset of 223 reference gages includes periods of record as early as 1891 and as recent as 2015, with an average period of record of 34 years and a range of 6 to 65 years.

2.3. Seasonal flow detection algorithm development

The following sections provide the theory and rationale for the Seasonal Flow Detection Algorithm (SFDA), explain the signal processing methods applied, and describe individual calculation steps. Additional description of signal processing methods is described in the Supplemental Materials.

2.3.1. Data smoothing

Data smoothing is a type of filtering in which low-frequency components are retained while high-frequency components are attenuated, enabling detection of features of interest at different frequencies or time-scales (Press and Teukolsky, 1990). Common finite-difference smoothing techniques include simple running averages, weighted moving averages, and exponential filters

(Janert, 2010). In this study, a Gaussian weighted moving average filter was used to generate a smoothed time series using the function gaussian_filter1d from the SciPy Image Processing package (Verveer, 2003) in Python. This smoothing method was selected for its ability to retain local maxima in the output function, while avoiding abrupt distortions in the filtered data. The Gaussian filter sets the weighting factors of the smoothing window w_j according to a Gaussian normal distribution

$$f(x,\sigma) = \frac{1}{\sqrt{2\pi\sigma^2}}\, exp\left(-\frac{1}{2}\left(\frac{x}{\sigma}\right)^2\right) \quad [1]$$

such that any new streamflow observation that enters the smoothing window is only gradually added to the moving average and then gradually removed. The standard deviation of the Gaussian function (σ) dictates the width of the distribution and consequently the degree of smoothing applied. In this study, low and high levels of streamflow data smoothing were associated with $\sigma < 5$ and $\sigma > 8$, respectively. For example, a daily streamflow time series smoothed with a high standard deviation Gaussian filter ($\sigma = 12$, Fig. 3) will dampen daily to weekly hydrologic variability while preserving major seasonal patterns. Alternatively, a low standard deviation Gaussian filter ($\sigma = 4$, Fig. 3) will preserve storm events occurring on weekly scales. High levels of smoothing are often applied first in the algorithm to identify coarse resolution temporal patterns such as the distinction between the annual wet and dry season, while removing the signal noise caused by individual storm events. Increasingly lower levels of smoothing are then applied to identify hydrologic features on finer temporal scales.

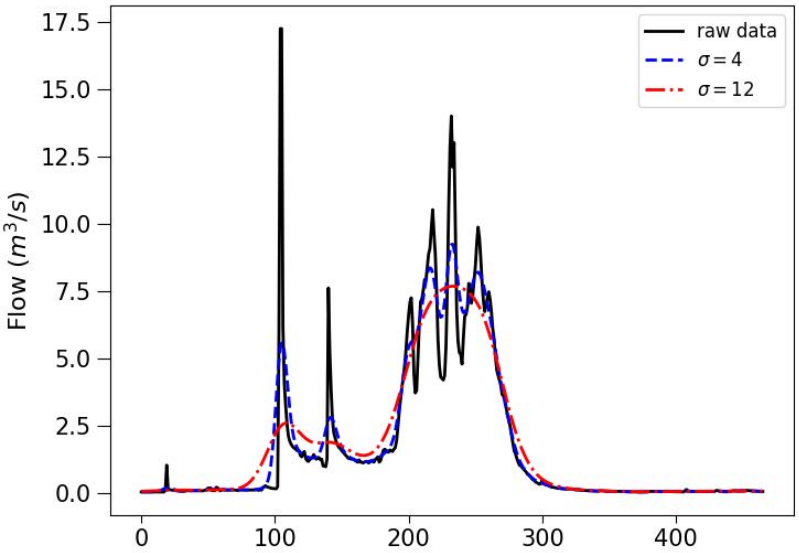

Fig. 3. Daily streamflow time series (black) plotted for one water year (Oct. 1–Sept. 30) with two levels of filters using Gaussian weighted moving averages with different σ parameter values.

2.3.2 Splines

Splines are functions constructed from segments of polynomials between each time series observation that are constrained to be smooth at the junctions (Letcher et al., 2001). Splines, which are used in the SFDA for derivative estimation of smoothed streamflow, have been shown to generate nearly optimal derivative estimates of noisy data such as streamflow time series due to low interpolation error (Craven and Wahba, 1979, Ragozin, 1983, Thomas et al., 2015). The SFDA employs a cubic spline function (three degrees of freedom) for derivative estimates, which is generally considered an optimal interpolation function for large time series (Carter and Signorino, 2010, Kimball, 1976, Wahba, 1978). For further explanation on spline fitting, refer to Hastie and Tibshirani (1990). In this study, derivative estimation using a cubic spline was performed on smoothed and windowed streamflow time series using the one-dimensional univariate spline fitting function available from the SciPy library in Python (Jones et al., 2001).

2.4. Seasonal flow detection algorithm (SFDA) general steps

The SFDA consists of six general steps used to detect seasonal flow transitions, although some applications may require either a subset of these steps or multiple iterations (Fig. 4). Steps are applied to each water year in a dataset, which in California is defined as October 1 to September 30. Step 1 (Fig. 4a): A high standard deviation Gaussian filter (G1) is applied to the observed daily streamflow time series to detect dominant peaks, valleys, or trends in the annual hydrograph. Depending on the level of smoothing, different frequency patterns (e.g., seasonal, sub-seasonal) are attenuated or left intact. Step 2 (Fig. 4b): A hydrologic feature of interest is identified from G1, such as annual peak flow. Step 3 (Fig. 4b): A localized search window is set around the feature of interest to constrain subsequent analysis to a hydrologically relevant period (e.g., 30 days before and after the feature of interest). Step 4 (Fig. 4c): Within the search window, a low standard deviation Gaussian filter (G2) is applied to the observed daily time series to extract high-resolution hydrologic patterns (e.g., individual storm events). Step 5 (Fig. 4d): A spline curve is fitted to smoothed data G2, and the derivative is taken to identify the slope of the hydrograph (S1'). Step 6 (Fig. 4d): A feature of interest is characterized in one of two ways: i) directly from G2 using relevant flow characteristics (i.e. magnitude), or ii) using the derivative of the spline curve (S1') to detect peaks or valleys of interest based on slope or sign change (triangles represent peak features of interest, and the black diamond is the final selected feature).

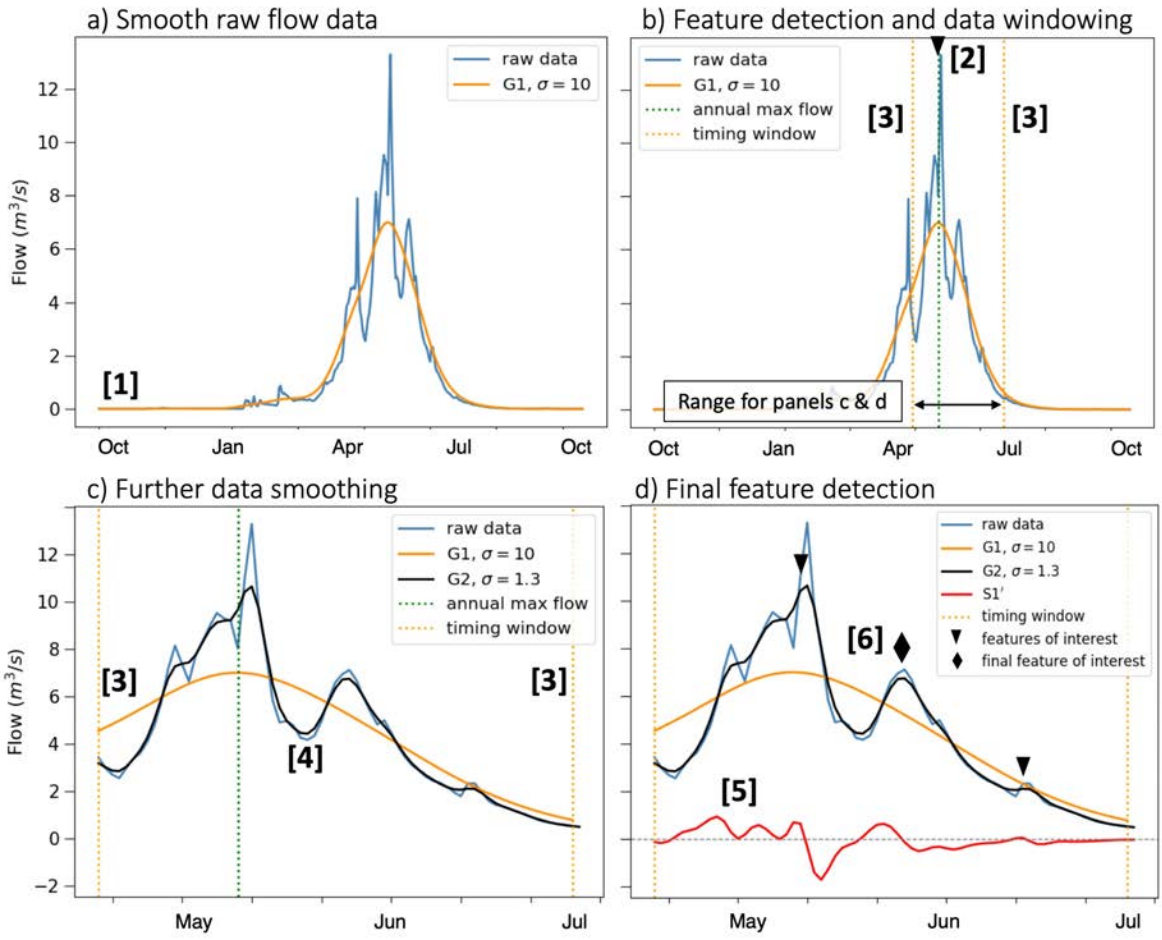

Fig. 4.Six general steps of the SFDA use data smoothing, windowing, and feature detection to identify seasonal flow transitions from daily streamflow data.

The SFDA steps are iterative and can be repeated multiple times to consistently and accurately identify flow transitions across water years and stream types. For example, the calculation of spring recession requires three iterations of smoothing and feature detection, while the calculation for dry season start timing only requires one iteration. The parameter values (e.g., smoothing parameter σ, window size, or magnitude thresholds) can be adjusted to suit the needs of particular flow regimes or hydrologic features of interest. For example, in flashy rain-driven streams the start of the dry season is generally indicated by the last significant storm event of the water year, which can be found using a low standard deviation Gaussian filter that closely fits daily streamflow data. Meanwhile, the start of

the dry season in a snowmelt-driven stream may be better identified by the general trend of flow reduction representing catchment drainage, which is best represented with a high standard deviation Gaussian filter to capture broader trends.

To contextualize the parameterization process, the algorithm for the dry season start timing may be considered. The dry season start timing is identified in the receding limb of the annual hydrograph through a combination of relative magnitude and slope, which are determined by parameterization. The start timing will be identified later in the water year, for example, if the relative magnitude threshold is reduced (requiring lower magnitude) or if the slope threshold is reduced (requiring a flatter slope), essentially creating more stringent hydrologic requirements. Further, the degree of smoothing applied to raw daily streamflow dampens fluctuations in flow and can allow a stabilized slope to be detected earlier in the water year as the level of smoothing is increased. The combinations of parameters for each algorithm were determined by expert opinion of the co-authors to best achieve timing of the functional flows illustrated conceptually in Fig. 1 across a diversity of hydrologic inputs, and this parameterization is available as default values in the SFDA code.

2.5. Application of the SFDA to functional flows in California

Four distinct applications of the SFDA were used to calculate the timing of functional flow component transitions based on reference-condition California streamflow gages (Fig. 2). In these applications, the SFDA steps were repeated up to three times to accurately identify functional flow transitions across the variety of stream types found in California. The parameter values (e.g., smoothing parameter σ or window size) were determined heuristically by the co-authors for each functional flow component to achieve timing results aligning with the conceptual timing of functional flow transitions illustrated in Fig. 1 and described in Yarnell et al. (2020). In the calibration process, parameters for each functional flow identification algorithm were empirically and incrementally adjusted to achieve hydrologically meaningful results; for example, the parameters for spring recession start timing (smoothing parameter σ, window sizes, and magnitude thresholds) were adjusted so that the timing would occur after wet season high flows, but before flows had receded to baseflow conditions. Supplemental Materials and associated online resources provide more information about the

calculation of each functional flow timing metric, how to download the SFDA code, and how to modify algorithm parameters to achieve desired results. To demonstrate SFDA application to a specific functional flow component, the calculation of wet season start timing is described in Section 2.5.1.

The timing metrics from the SFDA can be used to calculate additional functional flow metrics describing the magnitude, duration, frequency, and rate of change of flow within each functional flow component (e.g., baseflow magnitude or duration of the dry season) (Yarnell et al., 2020). The full suite of SFDA-based functional flow metrics can be visualized and downloaded at *eFlows.ucdavis.edu*, a website developed to view and interact with California's natural hydrology.

2.5.1. Functional flow calculation for wet season start timing

Wet season start timing delineates the portion of the water year during which streams receive the greatest inputs from storm runoff or snowmelt, and flows are elevated above dry season baseflow levels (Yarnell et al., 2020). The calculation for wet season start timing is presented as an example of the SFDA application to California functional flows. This calculation uses one iteration of the SFDA steps (Fig. 5). Within each water year, a high standard deviation Gaussian filter (G1, $\sigma = 10$) is applied (Fig. 5, Step 1) to detect the water year's global peak (P1) and preceding global valley (V1) (Fig. 5, Step 2). A relative magnitude threshold M1 is then set based on the magnitude of P1 and V1 as an upper limit ($M1 = \gamma*(P1-V1)$, where $\gamma = 0.2$), to ensure that the wet season start timing is not set after flows have already increased during the water year (Fig. 5, Step 3). A spline curve is fit to G1 so that its derivative can be used as a hydrologic requirement in the final feature detection step. Finally, searching backwards in time from P1, the date that discharge first falls below M1 and below a rate of change equaling ($\delta*P1$, where $\delta = 0.002$) is selected as the wet season start timing (Fig. 5, Step 4). The values for γ and δ were adjusted for California reference streamflow based on the co-authors' expert opinions to achieve identification of the functional flows described conceptually in Fig. 1 and Yarnell et al. (2020).

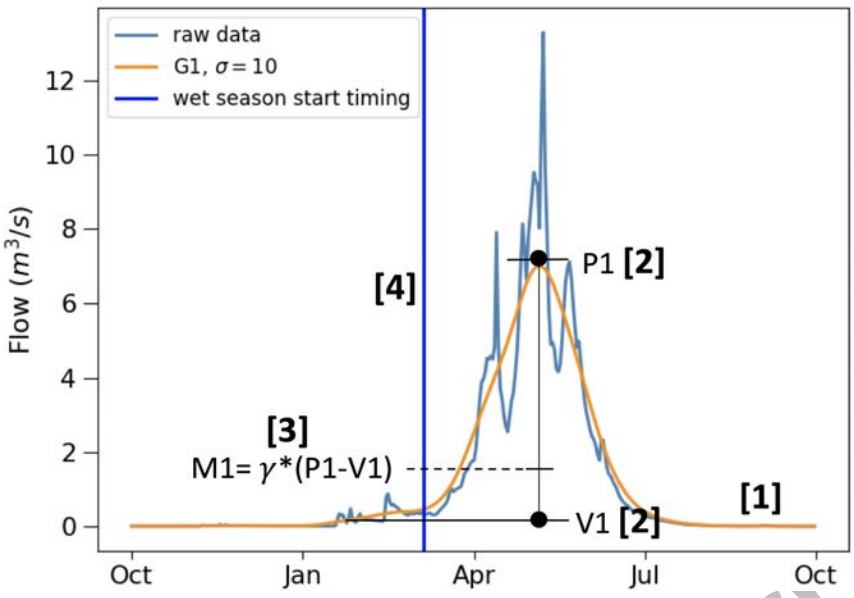

Fig. 5. SFDA steps to calculate the wet season start timing metric using data smoothing and feature detection based on magnitude and rate of change requirements.

2.6. Performance assessment

The calibrated SFDA was evaluated based on its ability to accurately determine the timing of functional flow transitions across all years in the California unimpaired streamflow dataset. The analyzed results consist of four flow timing metrics calculated annually for each gage (6–65 years per gage). Performance assessment included: 1) a comparison of results across stream types, 2) visual inspection of results, and 3) calculation of assessment indices to quantify issues in algorithm performance.

2.6.1. Comparison of functional flow timing results across stream types

Results were grouped by stream type (rain-, snowmelt-, or mixed rain and snowmelt-sourced) and visualized with violin plots, which use a rotated kernel density plot to depict the distribution of results. Distinct letters above the violin plots denote groups with statistically distinct mean values based on Tukey's Honestly Significant Difference statistical test with a confidence level of 95% (Abdi and Williams 2010). Groups with no statistical difference share the same letter above the violin plot.

Results were interpreted according to the co-authors' expert knowledge of California streamflow hydrology and supported where possible with relevant region-specific literature.

2.6.2. Visual performance assessment

Visual inspection of functional flow timing results was performed as a preliminary step to inform quantitative inspection (Section 2.6.3). The four annual flow timing metrics were reviewed for each water year in the dataset (n = 7475 years), yielding 29,900 visual inspections. Accuracy was visually assessed based on the authors' knowledge of California seasonal flow components and when they were expected to occur across a range of water year types. Results that appeared incorrect were tabulated, grouped according to functional flow component and stream type, and reviewed by multiple experts in California hydrology from the co-author team to ensure consistency. After performing the 29,900 visual inspections of the four timing metrics, issues were characterized based on the bias in timing (e.g., early or late timing) and the stream type in which it occurred.

2.6.3. Quantitative analysis with assessment indices

The purpose of this analysis was to quantify issues in algorithm performance observed during visual assessment. The issues characterized during visual assessment were quantified using programmed rules defined to identify occurrence of each issue across the dataset. For example, one rule identified years in rain-sourced streams in which dry season start timing was set after August 1. This was based on repeated observation that flow magnitude and slope generally decrease to baseflow levels in this stream type before August 1, and dry season start timing set after August 1 was usually inaccurate. The developed rules were quantified across relevant stream types and resulting values were termed assessment indices. Many of the assessment indices attempt to quantify cases in which functional flow timing was either earlier or later than expected for a given water year, and these issues with timing were often stream type-specific. For example, seasonal timing metrics tend to occur later in the water year for snowmelt-sourced streams than rain-sourced streams, so a dry season timing metric of March 1 could be considered anomalously early in snowmelt streams but normal in rain streams. Early or late occurrence was defined either through an empirical, evidence-based cut-off point (such as Aug. 1) or if possible through a relative hydrologic relationship, such as the number of high-flow events that occur before or after a particular timing metric is set. Other assessment indices quantify water year

features that make characterization with the SFDA difficult, such as dry water years in which only one or two peak flow events occur. Table 1 lists performance assessment indices used to quantify issues in algorithm timing calculations, based on final results from the SFDA.

3. Results and discussion

The SFDA was found to consistently identify functional flow components across a wide range of hydrologic input data, enabling quantitative differentiation across stream types based on the timing of seasonal functional flows. Example SFDA timing results are presented in Fig. 6 for individual water years spanning a range of stream types (rain-, mixed-, and snowmelt-sourced streams) and water year types (dry, moderate, and wet years) across a variety of watersheds, illustrating the ability of the SFDA to capture the timing of functional flow transitions in California across a diversity of hydrologic regimes.

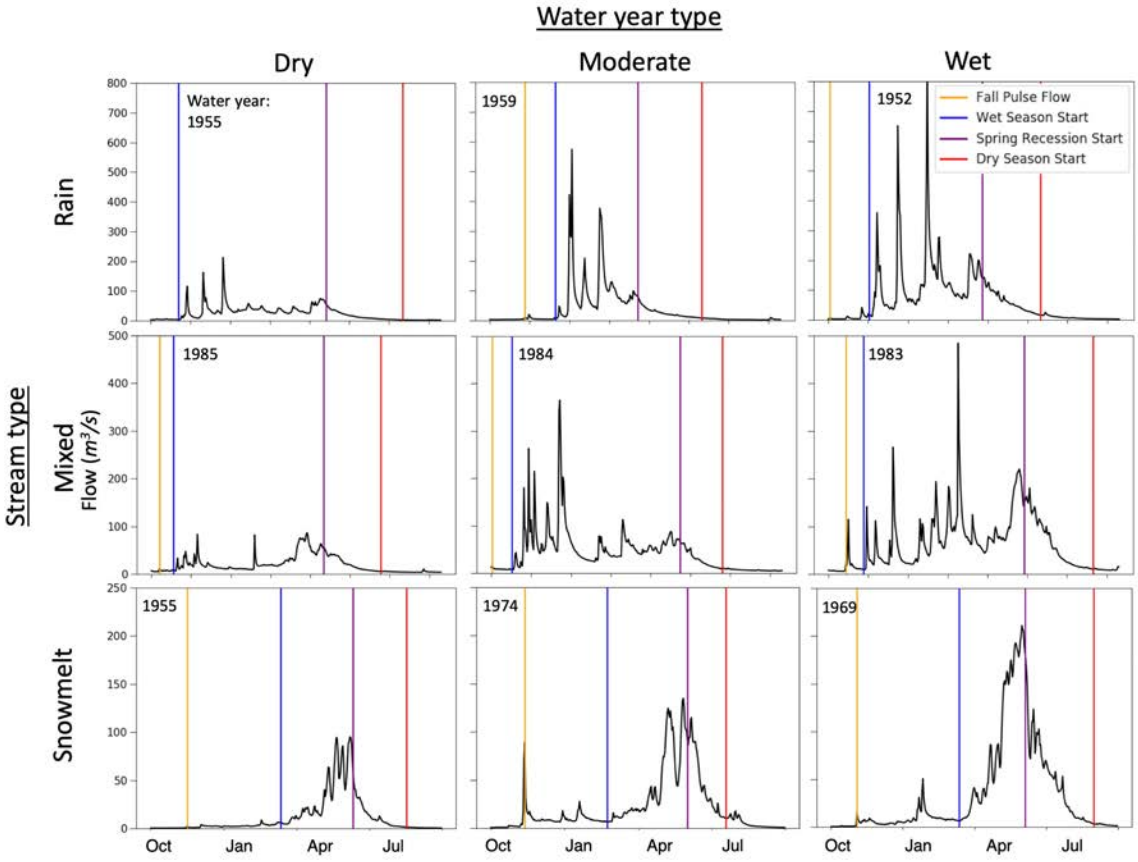

Fig. 6. Select SFDA results for the timing of functional flow transitions across three stream types (rain, mixed rain and snow, and snowmelt) and three water year types in California (dry, moderate, and wet). Individual hydrographs are from USGS gages 11529000 (rain), 11413100 (mixed rain and snow), and 11266500 (snowmelt).

3.1. Comparison of results across stream types

3.1.1. Fall pulse flow timing

The timing of the fall pulse flow marks the first peak flow of the water year when magnitude surpasses baseflow in a distinct pulse. Unlike the other functional flow components, the fall pulse flow is constrained to only occur during a subset time of the water year (Oct. 1-Dec. 15) when hydrologic requirements for relative magnitude and duration are met, and it does not necessarily occur in each water year. A fall pulse flow was identified in 60–65% of water years across all stream types. Although there were significant differences in event timing ($p < 0.05$) between snowmelt streams and other

stream types, wide overlap exists across all stream types (Fig. 7A). This is due in part to large-scale temperature and precipitation patterns that affect California streamflow. Early in the water year (Oct.-Nov.), temperatures across the state including the Sierra Nevada mountains are often above freezing, causing precipitation to fall as rain or rapidly melting snow (Lundquist et al., 2008, Serreze et al., 1999). Additionally, atmospheric river events can cause correlated streamflow patterns across much of the state (Cayan and Peterson, 1989), which are most pronounced when all precipitation is falling as rain. Therefore, a high degree of similarity is expected in the timing of fall pulse flows across all stream types. Further reason for the limited distinction among stream classes stems from the algorithm itself, which detects events over a narrow search window of 75 days (Oct.1-Dec. 15) considered ecologically significant for California streams (Yarnell et al., 2015). The upper and lower bounds of the violin plots span nearly the entire available time window of 75 days (Fig. 7A), indicating that fall pulse flow varies widely across all stream types. These results broadly align with Ahearn et al. (2004), who state that the season of flushing flows in California typically begins in November.

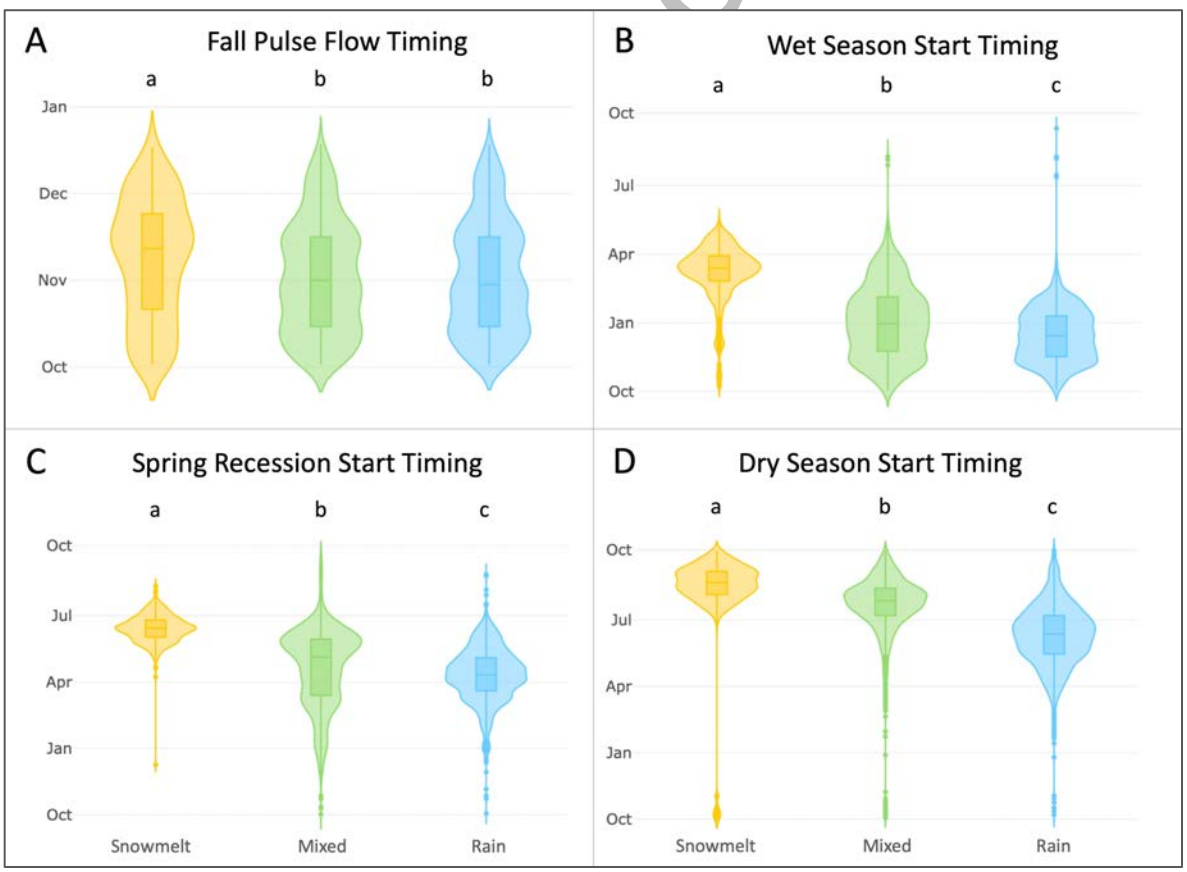

411 Fig. 7. Functional flow timing distributions across all stream types of California unimpaired streamflow.
412 Letters above violin plots indicate statistical significance. The y-axis spans the California water year
413 (Oct.-Sept. 31) for all components except the fall pulse flow, which is constrained from October 1-
414 December 15.
415
416 **3.1.2. Wet season start timing**
417 Wet season start timing is the date that the water year begins to experience consistently elevated
418 flows from either rainfall or snowmelt (Yarnell et al., 2020). The differences in these values were
419 statistically significant ($p < 0.05$) across the three stream types (Fig. 7B). The timing occurred three
420 to four months later in snowmelt-sourced streams (average Mar. 4) than rain-sourced streams
421 (average Dec. 12), and timing from mixed-source streams occurred across a wide range of values
422 whose mean (Dec. 30) closely resembles rain-sourced streams. These differences were expected due
423 to differing geographic and climatic drivers of wet season flow across California. In rain-sourced
424 streams, the timing of wet season flow closely reflects patterns of winter precipitation, which occurs
425 primarily during the winter months (Dec.-Feb.), although these peak flows also experience high
426 interannual variability in timing (Cayan and Peterson, 1989, Dettinger, 2011). In high elevation
427 snowmelt-sourced streams, peak flows are initiated by the snowmelt pulse as air temperatures warm
428 enough to melt snowpack in the spring. In mixed-source streams, wet season start timing may be
429 cued by either winter storms or a snowmelt pulse, resulting in a wide range of possible values driven
430 either by precipitation timing or temperature-driven snowmelt (Fig. 8). The proportion of streamflow
431 driven by rain versus snow is an important consideration in mid- and high-elevation basins, as runoff
432 is expected to shift towards more rain-driven flow with warming climate in the western United States
433 (Hamlet et al., 2005, Stewart et al., 2015, Sultana and Choi, 2018).

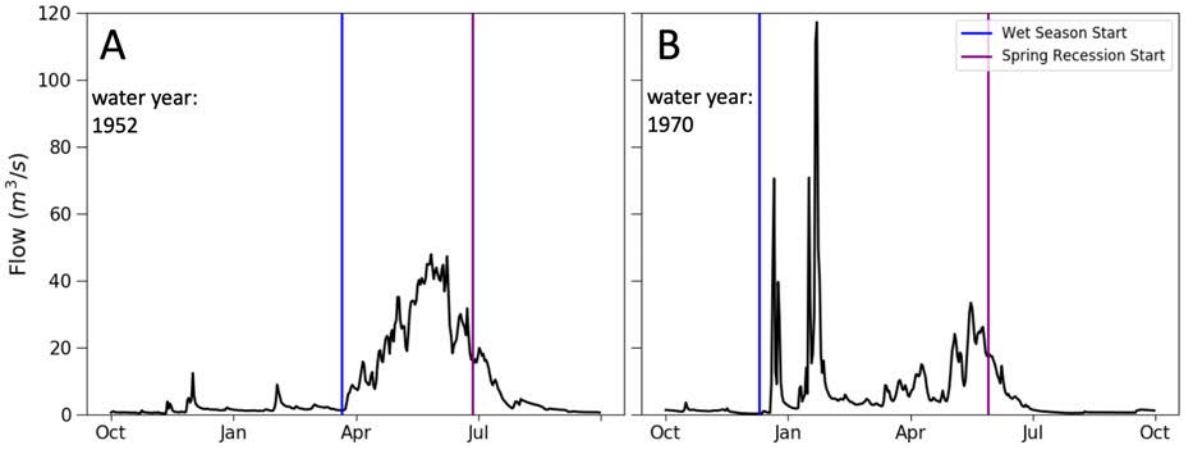

Fig. 8. Hydrographs of two different water years from a mixed-source stream (USGS gage 11414000) show varying contributions of snowmelt and winter rain storms, resulting in a wide range of results for spring recession start timing and wet season start timing.

3.1.3. Spring recession start timing

The spring recession represents the seasonal transition from wet season high flows to dry season low flows. The spring recession start timing is statistically distinct ($p < 0.05$) across the three California stream types, with timing occurring progressively later in the water year from rain-sourced to snowmelt-sourced streams (Fig. 7C). This distinction in timing is expected due to climatic influences on hydrology that shift as streams progress from lower to higher elevations and snowpack provides increasing amounts of storage that delay streamflow response to precipitation (Aguado et al., 1992). In California's highest elevations (above 2300 m), the spring recession is cued by a distinct temperature-driven snowmelt pulse. As the snowmelt influence diminishes and warming occurs earlier in lower elevation mixed-source streams (Fig. 2), the snowmelt pulse may arrive earlier or may not occur at all in dry years with very little snowpack relative to rainfall. In rain-sourced streams the spring recession is expected to occur after the last rain storm of the wet season, which tends to occur several months earlier in the year than the snowmelt pulse on average. The distribution of spring recession start timings in snowmelt-sourced streams is relatively narrow, with the majority of start dates occurring between May 23 and July 6 (average June 6), indicating predictable recession timing in snowmelt streams regardless of water year type (Yarnell et al., 2010).

455

456 The most variability in spring recession start timing occurs in mixed-source streams, which due to
457 their occurrence at mid-elevation regions are highly sensitive to changes in temperature and
458 snowpack (Lundquist et al., 2004, Stewart, 2008). Fig. 8 demonstrates how a greater snowmelt pulse
459 is associated with later spring recession timing, occurring 31 days later in water year 1952 than in
460 1970. This finding aligns with other research on streamflow in the western US, that has indicated both
461 temperature and annual flow volume are significant drivers of spring snowmelt runoff timing (Aguado
462 et al., 1992, Kormos et al., 2016). Adding to this variability, snowmelt-receiving streams in mid-
463 elevation regions of California have been subject to significant changes in the timing of snowmelt
464 recession peaks due to climate warming (Stewart, 2008). Hamlet et al. (2005) for example estimated
465 peak accumulation of snowmelt runoff in mid-elevation areas of California as occurring 15–45 days
466 earlier throughout the last century, which adds additional variation to the spring recession start timing
467 results in mixed snowmelt and rain regimes. Although rain-sourced streams also exhibit high
468 variability in spring recession timing, the average spring recession start timing across rain-sourced
469 streams (April 7) broadly aligns with the generally accepted end of the rainy season for California (Liu
470 et al., 2018).

471

472 **3.1.4. Dry season baseflow start timing**

473 The start timing of the dry season marks the beginning of the low flow, low variability portion of the
474 water year, in which the rate of recession flows has stabilized and magnitudes reach baseflow level.
475 Similar to spring recession start timing, dry season start timing is statistically distinct among the three
476 stream types ($p < 0.05$) and occurs gradually later on average from rain-sourced (June 6), to mixed-
477 source (July 16), to snowmelt-sourced streams (August 7) (Fig. 7D). The timing distribution ranges
478 more than 100 days in rain-sourced streams, which is consistent with the high inter-annual variability
479 of precipitation magnitude and timing (and consequently streamflow) exhibited in California (Dettinger
480 et al., 2011).

481

482 Despite high variability across rain-sourced streams, the average dry season start timing in these
483 streams is surprisingly consistent from small to large streams. For instance, the average dry season

start timing is June 8 in larger north coast streams (average annual flow 23 cms), and is similar in flashy ephemeral streams (average annual flow 0.5 cms), with an average start timing of May 27 (from Lane et al., 2017). However, interannual variability in dry season start timing within a single stream can be high, suggesting that central tendencies do not represent dry season timing conditions well in rain-sourced streams.

3.2. Performance assessment indices

Assessment indices were created to quantify the accuracy of the SFDA for identifying the timing of functional flow transitions in California reference streamflow. Assessment indices are presented in Table 1, and the following section highlights key issues and limitations for each functional flow. The frequency of most identified issues was less than 10%, except for Snow-early-wet and Mixed-early-spring, which are explained in Table 1 and below.

Table 1. Assessment indices for SFDA timing results.

Index name	Stream type	Issue	Assessment index calculation	Frequency
Fall-day1	All types	Fall pulse flow timing can occur on the very first day of the water year (Oct. 1), when it is difficult to determine from an annual hydrograph if the set date represents an actual peak or if it is capturing a recessing flow carried over from the previous water year.	Percentage of years in which the fall pulse timing is on day one of the water year (Oct. 1).	1%
Wet-season	All types	Occasionally the requirements for wet season start timing are not met so the metrics are not calculated.	Percentage of years in which spring recession or dry season start timing are calculated, but wet season start timing is not calculated.	2%
Spring-dry-gap	All types	A lag between spring recession and dry season start timing of more than five months indicates an anomaly within the water year, such as early spring recession or late dry season start timing, or a year in which the component timings were based off of a very limited number of storms.	Percentage of years in which the number of days between spring recession and dry season start timing is greater than 150 days (five months).	5%
Snow-late-spring	Snowmelt	Spring recession start timing can be calculated late into the recession period such that it occurs at the end of the snowmelt pulse instead of the beginning. Dry season start timing consequently occurs very soon after the spring recession timing.	Percentage of years in which spring recession start timing and dry season start timing occur within 21 days of each other.	1%
Snow-early-wet	Snowmelt	Wet season start timing in snowmelt streams can be triggered by large rainstorm	Percentage of years in which wet season start	25%

		flows early in the climatic wet season (Nov.-Jan.), and other years it is triggered by the snowmelt pulse (Apr.-May). This results in a wide range of start timing in the snowmelt stream type, triggered by differing hydrologic cues. Identification of timing before February 1 approximates how often wet season start timing is triggered by rainstorms instead of snowmelt.	timing occurs before February 1.	
Mixed-spring-wet/Rain-spring-wet	Mixed-source and Rain	In especially dry years, the annual hydrograph can be defined by a single large, brief storm event. This may cause wet season and spring recession start timing to be set based on a single storm such that they occur in close proximity.	Percentage of years in which wet season and spring recession start timing occur within 30 days of each other.	Mixed-spring-wet: 4%/ Rain-spring-wet: 4%
Mixed-early-spring/Rain-early-spring	Mixed-source and Rain	Spring recession start timing can occur before the end of wet season occurrence. This most commonly occurs in hydrographs without a strong snowmelt presence.	Percentage of years in which any high flows (>5th percentile) occur after that year's spring recession start date.	Mixed-early-spring: 21%/Rain-early-spring: 5%
Mixed-late-spring	Mixed-source	Dry season start timing can occur immediately after spring recession start timing, with a small gap of time between. This often occurs when the spring recession is identified too late into the period of receding high flows.	Percentage of years in which spring recession and dry season start timing occur within 21 days of each other.	1%
Rain-late-wet	Rain	Wet season start timing can occur late after the first high flows of the wet season.	Percentage of years in which any high flows (>5th percentile) occur before that year's wet season start date.	8%
Rain-late-dry	Rain	Dry season start timing can occur late into the dry season in rain-sourced streams, well after flows have already receded. This is usually the case when dry season start timing is set in August or later, based on repeated visual inspection.	Percentage of years in which dry season start timing occurs later than August 1.	10%

The methods presented here to identify hydrologic features and determine error differ from previous hydrologic studies, which can often take advantage of validated training sets to determine accuracy (Cannas et al., 2006, Letcher et al., 2001, Smith and Schwartz, 2017). The heuristic methods used in this research are similar to other approaches that require some subjectivity for parameterization of peak detection (Palshikar, 2009), and qualitative visual assessment methods are similar to approaches used to validate climate patterns in climate modeling studies that pair qualitative and quantitative model assessment (Gyalistras et al., 1994, Paul and Hsu, 2012). Performance assessment based on validation of known hydrologic conditions employed in this study is similar to the approach of Déry et al. (2009), who assessed a new method of spring recession identification across different river types in their study region. The proposed methods, although subjective in the choice of parametrization, present a consistent and repeatable way to identify functional flow components, advancing previous methods of quantifying seasonal streamflow patterns.

3.2.1. Issues in SFDA performance

Fig. 9 presents common issues in the SFDA for each functional flow component, which were often attributed to uncommon hydrologic patterns or effects from smoothing filters that occasionally have the undesired effect of over-dampening storm peaks while detecting broad hydrologic trends. In some water years, the first day of the water year (Oct.1) was identified as the date of the fall pulse flow, which presents ambiguity as to whether the first day of the water year is an actual peak event or is instead part of a continual decline from a peak in the previous water year (Fig. 9A). This situation occurs most often in naturalized gage data, with a 3.5% occurrence rate across all naturalized water years and an average occurrence rate of 1% across the entire dataset (Table 1, index WSI-day1).

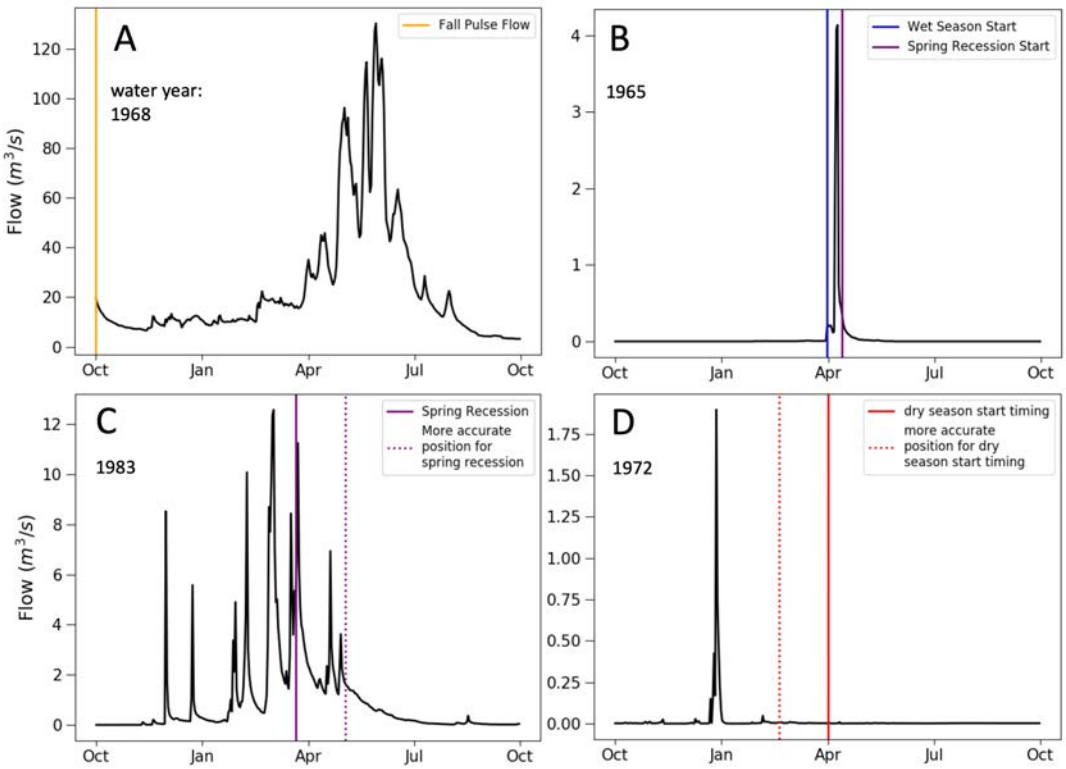

Fig. 9. Examples in which timing metrics are affected by uncommon hydrologic patterns (A and B) or are identified earlier or later than expected given expert understanding (C and D). Panels C and D illustrate the algorithm results compared to proposed improvements based on the co-authors'

526 understanding of California hydrology. Hydrographs from USGS gages 11213500 (A), 11046300 (B),
527 11033000 (C), and 11120520 (D).
528
529 Both mixed- and rain-sourced streams experienced some water years in which a single large high flow
530 event dominated the annual hydrograph such that start timings of wet season and spring recession
531 were based on the same peak flow (Fig. 9B). This occurred in 4% of mixed-source streams and 4% of
532 rain-sourced streams (Table 1, indices Mixed-spring-wet/Rain-spring-wet) and could result in
533 anomalous functional flow metrics based on these rare hydrologic conditions. In mixed-source
534 streams, early identification of spring recession start timing was found with a frequency of 21% (Table
535 1, index Mixed-early-spring), sometimes due to the effect of over-dampening rainstorm peaks with
536 smoothing filters when attempting to detect broad hydrologic trends (Fig. 9C). Conversely, spring
537 recession start timing occurred late in 10% of snowmelt stream water years, when the algorithm was
538 triggered by small peaks along the recession limb instead of the main snowmelt pulse (Table 1, index
539 Snow-early-spring). The algorithm for dry season start timing assesses the change in magnitude and
540 slope along the recession limb, so dry water years with very little change in these features are more
541 likely to have issues with component detection. This was often the case when dry season start timing
542 was identified late in the water year (Fig. 9D), which occurred in 10% of rain-sourced water years
543 (Table 1, index Rain-late-dry). These issues are expected to improve when SFDA parameters are
544 calibrated for smaller regions of streamflow data, instead of applying the same set of parameters
545 across a wide array of input data, as was done in this statewide case study.
546

4. Conclusions

This study developed an objective signal processing algorithm to address the need for a robust method to characterize the timing of seasonal flow transitions from daily streamflow time series. The Seasonal Flow Detection Algorithm (SFDA) improved on existing methods that rely on fixed time steps through the novel application of established signal processing techniques to identify the timing of seasonal flow transitions. The application to California streams demonstrated the ability of this approach to identify the timing of functional flow components from unimpaired daily streamflow time series across a wide range of climatic and geographic settings and extreme seasonal and interannual hydrologic variability. Results highlight hydrologic distinctions among varying drivers of streamflow, such as progressively later timing of spring recession flow as streams shift from rainfall-sourced to snowmelt-sourced flow regimes. Limitations of the approach were determined through a combination of visual expert-based assessment and quantitative performance assessment. In general, the percentage error in timing calculations did not exceed 10% across relevant water years for any assessment index, with infrequent exceptions. In a parallel effort, functional flow metrics produced by the SFDA for California reference gages are being extrapolated to ungaged streams to inform statewide environmental flow recommendations. Likewise, the SFDA has potential to be applied to other regions or countries sharing highly seasonal climates similar to California, by adjusting algorithm parameters to suit local hydrology. For instance, the SFDA metrics could be applied to assess shifts in streamflow due to climate change, with particular focus on potential changes in timing of seasonal flows. The proposed approach supports improved understanding of high-resolution spatial and temporal trends in hydrologic processes and climate conditions across complex landscapes and can inform environmental water management efforts.

CRediT authorship contribution statement

Noelle K. Patterson: Conceptualization, Software, Formal analysis, Methodology, Validation, Visualization, Writing - original draft, Writing - review & editing. **Belize A. Lane:** Conceptualization, Methodology, Supervision, Writing - original draft, Writing - review & editing. **Samuel Sandoval-Solis:** Conceptualization, Methodology, Supervision, Writing - review & editing. **Gregory B.**

Pasternack: Conceptualization, Writing - review & editing. **Sarah M. Yarnell:** Conceptualization, Writing - review & editing. **Yexuan Qiu:** Software.

Declaration of Competing Interest

The authors declare that they have no known competing financial interests or personal relationships that could have appeared to influence the work reported in this paper.

Acknowledgements

This work was supported by the UC Davis Hydrologic Sciences Graduate Group; the California State Water Resources Control Board [Grant number 16-062-300]; Utah Water Research Laboratory; and funding for G.B. Pasternack was provided by the USDA National Institute of Food and Agriculture [Hatch project number # CA-DLAW- 7034-H]. We thank Jason Hwan and two anonymous reviewers for improving the manuscript with insightful comments.

References

Aadland, L. (1993). Stream Habitat Types: Their Fish Assemblages and Relationship to Flow. *North American Journal of Fisheries Management*, *13*(4), 790–806. https://doi.org/10.1577/1548-8675(1993)013<0790:shttfa>2.3.co;2

Abatzoglou, J. T., Redmond, K. T., & Edwards, L. M. (2009). Classification of Regional Climate Variability in the State of California. Journal of Applied Meteorology and Climatology, 48, 1527–1541. https://doi.org/10.1175/2009JAMC2062.1

Abdi, H., & Williams, L. J. (2010). Tukey' s Honestly Significant Difference (HSD) Test. In Encyclopedia of Research Design (pp. 1–5). Thousand Oaks, CA: Sage.

595 Adamowski, J., & Sun, K. (2010). Development of a coupled wavelet transform and neural network
596 method for flow forecasting of non-perennial rivers in semi-arid watersheds. *Journal of*
597 *Hydrology*, *390*(1–2), 85–91. https://doi.org/10.1016/j.jhydrol.2010.06.033

598 Aguado, E., Cayan, D., Riddle, L., & Roos, M. (1992). Climatic Fluctuations and the Timing of West
599 Coast Streamflow. Journal of Climate, 5, 1468–1483.

600 Ahearn, D. S., Sheibley, R. W., Dahlgren, R. A., & Keller, K. E. (2004). Temporal dynamics of
601 stream water chemistry in the last free-flowing river draining the western Sierra Nevada,
602 California. *Journal of Hydrology*, *295*(1–4), 47–63. https://doi.org/10.1016/j.jhydrol.2004.02.016

603 Bart, R., & Hope, A. (2014). Inter-seasonal variability in baseflow recession rates: The role of aquifer
604 antecedent storage in central California watersheds. *Journal of Hydrology*, *519*, 205–213.
605 https://doi.org/10.1016/j.jhydrol.2014.07.020

606 Booker, D. J., & Acreman, M. C. (2007). Generalisation of physical habitat-discharge relationships.
607 *Hydrology and Earth System Sciences*, *11*(1), 141–157.

608 Buttle, J. M. (2011). Streamflow response to headwater reforestation in the Ganaraska River basin,
609 southern Ontario, Canada. *Hydrological Processes*, *25*, 3030–3041.
610 https://doi.org/10.1002/hyp.8061

611 Cambray, J. A. (1991). The effects on fish spawning and management implications of impoundment
612 water releases in an intermittent South African river. *Regulated Rivers: Research &*
613 *Management*, *6*(1), 39–52. https://doi.org/10.1016/j.otc.2010.04.018

614 Cannas, B., Fanni, A., See, L., & Sias, G. (2006). Data preprocessing for river flow forecasting using
615 neural networks: Wavelet transforms and data partitioning. *Physics and Chemistry of the*
616 *Earth*, *31*(18), 1164–1171. https://doi.org/10.1016/j.pce.2006.03.020

617 Carter, D. B., & Signorino, C. S. (2010). Back to the Future : Modeling Time Dependence in Binary
618 Data. *Political Analysis*, *18*, 271–292. https://doi.org/10.1093/pan/mpq013

Cayan, D. R., & Peterson, D. H. (1989). The Influence of North Pacific Atmospheric Circulation on Streamflow in the West. *Geophysical Monograph*, *55*, 375–397.

CDWR (California Department of Water Resources), 2007. *California Central Valley Unimpaired Flow Data*. (2007). Bay-Delta Office; California Department of Water Resources. Sacramento; California. http://www.waterboards.ca.gov/waterrights/water_issues/programs/bay_delta/bay_delta_plan/water_quality_control_plan

Cleaveland, W. S., & Loader, C. (1996). Smoothing by Local Regression: Principles and Methods. In *Statistical theory and computational aspects of smoothing* (pp. 10–49). Physica-Verlag HD. https://doi.org/10.2307/1271204

Craven, P., & Wahba, G. (1979). Smoothing noisy data with spline functions - Estimating the correct degree of smoothing by the method of generalized cross-validation. *Numerische Mathematik*, *31*(4), 377–403. https://doi.org/10.1007/BF01404567

Dettinger, M. (2011). Climate change, atmospheric rivers, and floods in California - a multimodel analysis of storm frequency and magnitude changes. *Journal of the American Water Resources Association*, *47*(3), 514–523. https://doi.org/10.1111/j.1752-1688.2011.00546.x

Dettinger, M. D., Ralph, F. M., Das, T., Neiman, P. J., & Cayan, D. R. (2011). Atmospheric Rivers, Floods and the Water Resources of California. *Water*, *3*(4), 445–478. https://doi.org/10.3390/w3020445

Déry, S. J., Stahl, K., Moore, R. D., Whitfield, P. H., Menounos, B., & Burford, J. E. (2009). Detection of runoff timing changes in pluvial, nival, and glacial rivers of western Canada. *Water Resources Research*, *45*, 1–11. https://doi.org/10.1029/2008WR006975

Escobar-Arias, M. I., & Pasternack, G. B. (2010). A hydrogeomorphic dynamics approach to assess in-stream ecological functionality using the functional flows model, part 1—model characteristics. *River Research and Applications*, *26*(9), 1103–1128. https://doi.org/10.1002/rra.1316

644 Falcone, J. A., Carlisle, D. M., Wolock, D. M., & Meador, M. R. (2010). GAGES : A stream gage
645 database for evaluating natural and altered flow conditions in the conterminous United States.
646 *Ecology*, *91*(2), 621.

647 Gasith, A., & Resh, V. H. (1999). Streams in Mediterranean Climate Regions: Abiotic Influences and
648 Biotic Responses to Predictable Seasonal Events. *Annual Review of Ecology and Systematics*,
649 *30*, 51–81. https://doi.org/10.1146/annurev.ecolsys.30.1.51

650 Greet, J., Webb, J. A., & Cousens, R. D. (2011). The importance of seasonal flow timing for riparian
651 vegetation dynamics: a systematic review using causal criteria analysis. Freshwater Biology,
652 56, 1231–1247. https://doi.org/10.1111/j.1365-2427.2011.02564.x

653 Gyalistras, D., Storch, H. Von, Fischlin, A., & Beniston, M. (1994). Linking GCM-simulated climatic
654 changes to ecosystem models: case studies of statistical downscaling in the Alps. Climate
655 Research, 4, 167–189.

656 Hall, F. R. (1968). Base-Flow Recessions—A Review. *Water Resources Research*, *4*(5), 973–983.
657 https://doi.org/10.1029/WR004i005p00973

658 Hamlet, A. F., Mote, P. W., Clark, M. P., & Lettenmaier, D. P. (2005). Effects of temperature and
659 precipitation variability on snowpack trends in the Western United States. *Journal of Climate*,
660 *18*(21), 4545–4561. https://doi.org/10.1175/JCLI3538.1

661 Hastie, T. J., & Tibshirani, R. (1990). *Generalized Additive Models*. Chapman and Hall.

662 Henriksen, B. J. A., Heasley, J., Kennen, J. G., & Nieswand, S. (2006). *Users' Manual for the*
663 *Hydroecological Integrity Assessment Process Software (including the New Jersey*
664 *Assessment Tools)*.

665 Jacobson, R. B. (2013). Riverine Habitat Dynamics. In J. J. Shroder, D. Butler, & C. Hupp (Eds.),
666 *Treatise on Geomorphology* (pp. 6–19). San Diego, CA: Academic Press.
667 https://doi.org/10.1016/B978-0-12-374739-6.00318-3

668 Janert, P. K. (2010). *Data Analysis with Open Source Tools* (1st ed.). O'Reilly Media, Inc.

669 Jones, E., Oliphant, T., & Peterson, P. (2001). SciPy: Open source scientific tools for Python.
670 Online; accessed 2017-09-21. Retrieved from http://www.scipy.org/

671 Kennard, M. J., Mackay, S. J., Pusey, B. J., Olden, J. D., & Nick, M. (2010). Quantifying Uncertainty
672 in Estimation of Hydrologic Metrics for Ecohydrological Studies. *River Research and*
673 *Applications*, *26*, 137–156. https://doi.org/10.1002/rra.1249

674 Kimball, B. A. (1976). Smoothing Data with Cubic Splines. *Agronomy Journal*, *68*, 126–129.

675 Kormos, P. R., Luce, C. H., Wegner, S. J., & Berghuijs, W. R. (2016). Trends and sensitivities of low
676 streamflow extremes to discharge timing and magnitude in Pacific Northwest mountain
677 streams. Water Resources Research, 52, 4990–5007. https://doi.org/10.1002/2015WR018125.

678 Kusche, J., Schmidt, R., Petrovic, S., & Rietbroek, R. (2009). Decorrelated GRACE time-variable
679 gravity solutions by GFZ, and their validation using a hydrological model. *Journal of Geodesy*,
680 *83*, 903–913. https://doi.org/10.1007/s00190-009-0308-3

681 LaDochy, S., Medina, R., & Patzert, W. (2007). Recent California climate variability: spatial and
682 temporal patterns in temperature trends. Climate Research, 33, 159–169.

683 Lane, B. A., Dahlke, H. E., Pasternack, G. B., & Sandoval-Solis, S. (2017). Revealing the Diversity
684 of Natural Hydrologic Regimes in California with Relevance for Environmental Flows
685 Applications. *Journal of the American Water Resources Association*, *53*(2), 411–430.
686 https://doi.org/10.1111/1752-1688.12504

687 Lane, B. A., Sandoval-solis, S., Stein, E. D., Yarnell, S. M., Pasternack, G. B., & Dahlke, H. E.
688 (2018). Beyond metrics? The role of hydrologic baseline archetypes in environmental water
689 management. *Environmental Management*, *62*(4), 678–693. https://doi.org/10.1007/s00267-
690 018-1077-7

Letcher, R. A., Yu Schreider, S., Jakeman, A. J., Neal, B. P., & Nathan, R. J. (2001). Methods for the analysis of trends in streamflow response due to changes in catchment condition. *Environmetrics*, *12*(7), 613–630. https://doi.org/10.1002/env.486

Liu, Y. C., Di, P., Chen, S. H., & DaMassa, J. (2018). Relationships of rainy season precipitation and temperature to climate indices in California: Long-Term variability and extreme events. *Journal of Climate*, *31*(5), 1921–1942. https://doi.org/10.1175/JCLI-D-17-0376.1

Lundquist, J. D., Cayan, D. R., & Dettinger, M. D. (2004). Spring Onset in the Sierra Nevada: When Is Snowmelt Independent of Elevation? Journal of Hydrometeorology, 5, 327–342.

Lundquist, J. D., Neiman, P. J., Martner, B., White, A. B., Gottas, D. J., & Ralph, F. M. (2008). Rain versus Snow in the Sierra Nevada, California: Comparing Doppler Profiling Radar and Surface Observations of Melting Level. *Journal of Hydrometeorology*, *9*(2), 194–211. https://doi.org/10.1175/2007jhm853.1

Mann, M. E. (2004). On smoothing potentially non-stationary climate time series. *Geophysical Research Letters*, *31*(January), 18–21. https://doi.org/10.1029/2004GL019569

Mazor, R. D., May, J. T., Sengupta, A., McCune, K. S., Bledsoe, B. P., & Stein, E. D. (2017). Tools for managing hydrologic alteration on a regional scale: Setting targets to protect stream health. *Freshwater Biology*, 786–803. https://doi.org/10.1111/fwb.13062

Mount, J. F. (1995). *California Rivers and Streams: The Conflict Between Fluvial Process and Land Use*. Berkeley: University of California Press.

Olden, J. D., & Poff, N. L. (2003). Redundancy and the choice of hydrologic indices for characterizing streamflow regimes. *River Research and Applications*, *19*(2), 101–121. https://doi.org/10.1002/rra.700

Palshikar, G. (2009). Simple Algorithms for Peak Detection in Time- Series Simple Algorithms for Peak Detection in Time-Series. In *Proc. 1st Int. Conf. Advanced Data Analysis, Business Analytics and Intelligence*.

716 Pasternack, G. B., & Hinnov, L. A. (2003). Hydrometeorological controls on water level in a
717 vegetated Chesapeake Bay tidal freshwater delta, *58*, 367–387. https://doi.org/10.1016/S0272-
718 7714(03)00106-9

719 Paul, S., & Hsu, H.-H. (2012). Comparative Study of Performance of CMIP3 GCMs in Simulating the
720 East Asian Monsoon Variability. Terrestrial, Atmospheric and Oceanic Sciences, 23(4), 377–
721 395. https://doi.org/10.3319/TAO.2012.02.01.01(A)1.

722 Poff, N. L., Allan, J. D., Bain, M. B., Karr, J. R., Prestegaard, K. L., Richter, B. D., … Stromberg, J.
723 C. (1997). The natural flow regime. *Bioscience*, *47*(11), 769–784. https://doi.org/Doi
724 10.2307/1313099

725 Poff, N. L., & Ward, J. V. (1989). Implications of Streamflow Variability and Predictability for Lotic
726 Community Structure: A Regional Analysis of Streamflow Patterns. *Canadian Journal of*
727 *Fisheries and Aquatic Sciences*, *46*(10), 1805–1818. https://doi.org/10.1139/f89-228

728 Poff, N. L., & Zimmerman, J. K. H. (2010). Ecological responses to altered flow regimes: a literature
729 review to inform the science and management of environmental flows. *Freshwater Biology*,
730 *55*(1), 194–205. https://doi.org/10.1111/j.1365-2427.2009.02272.x

731 Pollock, D. S. G. (1999). *A Handbook of Time-Series Analysis, Signal Processing and Dynamics*.
732 London: The Academic Press. https://doi.org/https://doi.org/10.1016/B978-0-12-560990-
733 6.X5000-3

734 Press, W. H., & Teukolsky, S. A. (1990). Savitzky-Golay Smoothing Filters. *Computers in Physics*,
735 *4*(669). https://doi.org/10.1063/1.4822961

736 Ragozin, D. L. (1983). Error bounds for derivative estimates based on spline smoothing of exact or
737 noisy data. *Journal of Approximation Theory*, *37*(4), 335–355. https://doi.org/10.1016/0021-
738 9045(83)90042-4

739 Richter, B. D., Baumgartner, J. V., Powell, J., & Braun, D. P. (1996). A Method for Assessing
740 Hydrologic Alteration within Ecosystems. *Conservation Biology*, *10*(4).

741 Rood, S. B., Samuelson, G. M., Braatne, J. H., Gourley, C. R., Hughes, F. M. R., Mahoney, J. M., &
742 Hughes, F. (2005). Managing river flows to restore floodplain forests. *Frontiers in Ecology and*
743 *the Environment*, *3*(4), 193–201.

744 Sang, Y. F. (2013). A review on the applications of wavelet transform in hydrology time series
745 analysis. *Atmospheric Research*, *122*, 8–15. https://doi.org/10.1016/j.atmosres.2012.11.003

746 Sawaske, S. R., & Freyberg, D. L. (2014). An analysis of trends in baseflow recession and low-flows
747 in rain-dominated coastal streams of the pacific coast. *Journal of Hydrology*, *519*(PA), 599–
748 610. https://doi.org/10.1016/j.jhydrol.2014.07.046

749 Schneider, R. (2011). *Survey of Peaks / Valleys identification in Time Series*.

750 Scholkmann, F., Boss, J., & Wolf, M. (2012). An Efficient Algorithm for Automatic Peak Detection in
751 Noisy Periodic and Quasi-Periodic Signals. *Algorithms*, *5*, 588–603.
752 https://doi.org/10.3390/a5040588

753 Serreze, M. C., Clark, M. P., Armstrong, R. L., McGinnis, D. A., & Pulwarty, R. S. (1999).
754 Characteristics of the western United States snowpack from snowpack telemetry (SNOTEL)
755 data. *Water Resources Research*, *35*(7), 2145–2160. https://doi.org/10.1029/1999wr900090

756 Smith, B, Schwartz, S, 2017. Automating Recession Curve Displacement Recharge
757 Estimation. Groundwater 55 (1), 81–87. doi:10.1111/gwat.12439. In press.

758 Stewart, I. T. (2008). Changes in snowpack and snowmelt runoff for key mountain regions.
759 *Hydrological Processes*, *23*(1), 78–94. https://doi.org/10.1002/hyp.7128

760 Stewart, I. T., Ficklin, D. L., Carrillo, C. A., & Mcintosh, R. (2015). 21st century increases in the
761 likelihood of extreme hydrologic conditions for the mountainous basins of the Southwestern
762 United States. *Journal of Hydrology*, *529*, 340–353
763 https://doi.org/10.1016/j.jhydrol.2015.07.043

764 Sultana, R., & Choi, M. (2018). Sensitivity of Streamflow Response in the Snow-Dominated Sierra
765 Nevada Watershed Using Projected CMIP5 Data. *Journal of Hydrologic Engineering*, *23*(8), 1–
766 12. https://doi.org/10.1061/(ASCE)HE.1943-5584.0001640.

767 Thomas, B. F., Vogel, R. M., & Famiglietti, J. S. (2015). Objective hydrograph baseflow recession
768 analysis. *Journal of Hydrology*, *525*, 102–112. https://doi.org/10.1016/j.jhydrol.2015.03.028

769 Verveer, P. J. (2003). SciPy Reference Guide: Multi-dimensional image processing - "gaussian
770 filter1d" and "gaussian filter."

771 Wahba, G. (1978). Improper Priors , Spline Smoothing and the Problem of Guarding Against Model
772 Errors in Regression. *Journal of the Royal Statistical Society. Series B (Methodological).*,
773 *40*(3), 364–372.

774 Yarnell, S. M., Viers, J. H., & Mount, J. F. (2010). Ecology and Management of the Spring Snowmelt
775 Recession. *BioScience*, *60*(2), 114–127. https://doi.org/10.1525/bio.2010.60.2.6

776 Yarnell, S. M., Petts, G. E., Schmidt, J. C., Whipple, A. A., Beller, E. E., Dahm, C. N., … Viers, J. H.
777 (2015). Functional Flows in Modified Riverscapes: Hydrographs, Habitats and Opportunities.
778 *BioScience*, *65*(10), 963–972. https://doi.org/10.1093/biosci/biv102

779 Yarnell, S. M., Stein, E. D., Webb, J. A., Grantham, T., Lusardi, R. A., Zimmerman, J., … Sandoval-
780 Solis, S. (2020). A functional flows approach to selecting ecologically relevant flow metrics for
781 environmental flow applications. *River Research and Applications*, *36*(2), 1–7.
782 https://doi.org/10.1002/rra.3575

783 Zhang, H., Huang, Q., Zhang, Q., Gu, L., Chen, K., & Yu, Q. (2016). Changes in the long-term
784 hydrological regimes and the impacts of human activities in the main. *Hydrological Sciences*
785 *Journal*, *61*(6), 1054–1068. https://doi.org/10.1080/02626667.2015.1027708

786 Zimmerman, J. K. H., Carlisle, D. M., May, J. T., Klausmeyer, K. R., Grantham, T. E., Brown, L. R.,
787 & Howard, J. K. (2017). Patterns and magnitude of flow alteration in California , USA.
788 *Freshwater Biology*, 859–873. https://doi.org/10.1111/fwb.13058

789

790